

Facile Synthesis and Tensile Behavior of TiO₂ One-Dimensional Nanostructures

Syed S. Amin · Shu-you Li · Xiaoxia Wu ·
Weiqiang Ding · Terry T. Xu

Received: 23 August 2009 / Accepted: 28 October 2009 / Published online: 18 November 2009
© to the authors 2009

Abstract High-yield synthesis of TiO₂ one-dimensional (1D) nanostructures was realized by a simple annealing of Ni-coated Ti grids in an argon atmosphere at 950 °C and 760 torr. The as-synthesized 1D nanostructures were single crystalline rutile TiO₂ with the preferred growth direction close to [210]. The growth of these nanostructures was enhanced by using catalytic materials, higher reaction temperature, and longer reaction time. Nanoscale tensile testing performed on individual 1D nanostructures showed that the nanostructures appeared to fracture in a brittle manner. The measured Young's modulus and fracture strength are ~56.3 and 1.4 GPa, respectively.

Keywords TiO₂ nanomaterials ·
Synthesis and characterization · Nanoscale tensile testing

Introduction

Titanium dioxide (TiO₂) one-dimensional (1D) nanostructures have received extensive research attention recently because of their promising applications in photo-catalysis,

gas and humidity sensing, solar water splitting, bio-scaffolds, and others [1–3]. Both “wet-chemistry” and “dry” synthetic methods have been used to prepare TiO₂ 1D nanostructures. The “wet-chemistry” methods such as sol-gel process and anodic oxidation require further heat treatment to improve the crystallinity of as-synthesized nanostructures, which adds to the complexity of the processes. A few “dry” synthetic methods including vapor transport, metal-organic chemical vapor deposition (MOCVD), and annealing have been reported. The vapor transport method involves thermal evaporation of titanium (Ti) sources (e.g., Ti or TiO powders), transport of Ti-containing vapors, and final growth of TiO₂ nanostructures on Ti-coated substrates [4–6]. This method requires precise control of source temperatures and reaction temperatures, which can be experimentally challenging. The MOCVD method can grow well-aligned TiO₂ 1D nanostructures [7, 8]. However, the MOCVD system setup is complicated and expensive. The annealing method grows TiO₂ 1D nanostructures by direct oxidation of Ti foils using acetone, ethanol, or dibutyltin dilaurate (DBTDL) vapor as oxygen (O₂) sources [9–11]. While this method is relatively simple, the use of organic vapor could introduce carbon contamination and result in the growth of TiO₂ core-amorphous carbon shell structures [10]. Thus, it is necessary to seek simpler and more reliable “dry” synthetic methods to synthesize high quality TiO₂ 1D nanostructures. In addition, since mechanical stability is a crucial factor for structural integrity for the intended applications of TiO₂ nanostructures, it is important to study the mechanical properties of individual TiO₂ 1D nanostructures.

In our previous work, a facile approach to synthesize TiO₂ 1D nanostructures by direct heating of nickel (Ni)-coated TiO powders was demonstrated [12]. In this work, an even simpler one-step “dry” synthetic approach is reported,

S. S. Amin · X. Wu · T. T. Xu (✉)
Department of Mechanical Engineering and Engineering
Science, The University of North Carolina at Charlotte,
Charlotte, NC 28223, USA
e-mail: ttxu@uncc.edu

S. Li
NUANCE Center, Northwestern University,
Evanston, IL 60208, USA

W. Ding (✉)
Department of Mechanical and Aeronautical Engineering,
Clarkson University, Potsdam, NY 13699, USA
e-mail: wding@clarkson.edu

which produces single crystalline rutile TiO_2 1D nanostructures by direct heating of Ni-coated Ti grids in an argon (Ar) environment at the atmospheric pressure. The mechanical properties of individual nanostructures were studied by a nanoscale tensile testing method using a custom-made nanomanipulator inside the vacuum chamber of a scanning electron microscope. According to the knowledge of the authors, this is the first time that the tensile behavior of rutile TiO_2 1D nanostructures is reported.

Materials Synthesis and Characterization

Single crystalline rutile TiO_2 1D nanostructures were synthesized by annealing catalytic material-coated Ti grids in Ar at the atmospheric pressure. Typical synthetic conditions are described in this paragraph, whereas conditions used in control experiments (e.g., variation of reaction temperatures) will be described later. Briefly, commercial Ti grids (Structure Probe Inc; mesh size varies from 100 to 400 mesh) were used as the starting material without any further cleaning procedures. A thin film of Ni (~ 2 nm) was deposited on Ti grids by magnetron sputtering (Denton Vacuum: Desk[®] IV TSC). Ni-coated Ti grids were then loaded into a quartz boat and placed in the desired position inside a quartz tube (ϕ : 1 in. diameter) of a home-built horizontal tube furnace system. The system was first evacuated to ~ 10 mTorr and then brought back to the atmospheric pressure (~ 760 Torr) with Ar (Linde: 99.999% UHP). A continuous flow of 10 sccm (standard cubic centimeter per minute) Ar was then introduced and maintained for the rest of experiment. The quartz tube was ramped up to 950°C (center position temperature measured outside the quartz tube by a thermocouple) in 60 min and soaked at that temperature for 30 min, followed by cooling down to room temperature in ~ 4 h. The Ti grids were then taken out and characterized by scanning electron microscopy (SEM) (JEOL JSM-6480), transmission electron microscopy (TEM; JEOL JEM-2100F) including electron energy loss spectroscopy (EELS) and selected area electron diffraction (SAED), X-ray diffraction (XRD; PANalytical X'Pert Pro diffractometer), and micro-Raman spectroscopy (Reinshaw RM 2000 confocal micro-Raman system in the back-scattering configuration; 514.5 nm excitation green laser).

Figure 1a, b is low and high magnification SEM images of as-synthesized 1D nanostructures grown on a 400 mesh Ti grid, respectively. Uniformly distributed nanostructures consisting of both wire- and belt-like morphologies can be found all over the grid. These nanostructures are 20–80 nm in width and 5–20 μm in length. Figure 1c is the micro-Raman spectrum revealing three major peaks at ~ 224 , 444, and 607 cm^{-1} . These peaks match closely to the reference values for rutile TiO_2 [13]. Figure 1d is the XRD

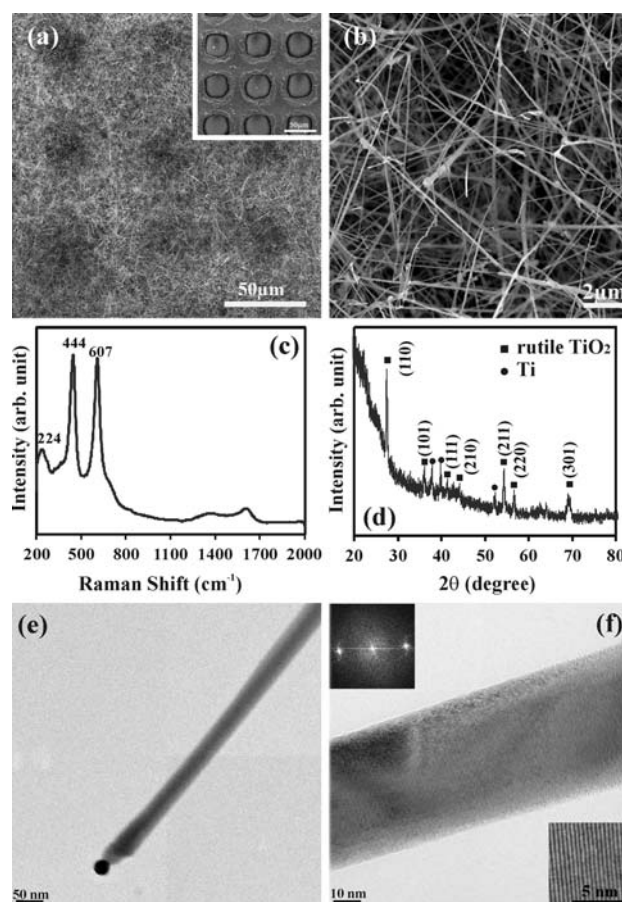


Fig. 1 SEM images of as-synthesized nanostructures on a Ti grid recorded at low (a) and high (b) magnifications, respectively. The inset in a shows a bare Ti grid before reaction. c A micro-Raman spectrum shows three peaks at 224, 444, and 607 cm^{-1} , corresponding to the Raman active modes B_{1g} , E_g and A_{1g} of rutile TiO_2 , respectively. d A XRD spectrum shows diffraction peaks, most of which could be indexed to rutile TiO_2 . The higher intensity background recorded before the (110) peak was contributed from the glass slide used to hold the samples. e A low magnification TEM image shows a catalytic material on the tip of a nanostructure. f A high magnification TEM image shows a part of one nanostructure. The FFT pattern demonstrates the single crystalline nature of the nanostructure. The lattice fringes in the inset have a neighboring spacing of 0.358 nm, close to the d -spacing of (110) plane of rutile TiO_2 . The growth direction of the nanostructure is close to the [210] direction

spectrum whose most diffraction peaks can be indexed to the rutile TiO_2 according to the JCPDS card No. 21-1276 [14]. TEM/EELS/diffraction pattern analyses revealed that the nanostructures are single crystalline, and most of them have the catalytic material Ni on their tips. Figure 1e is a low magnification TEM image, showing a 1D nanostructure with a catalytic particle on its tip. Figure 1f is a high magnification TEM image of a part of a 1D nanostructure. The corresponding fast Fourier transform (FFT) pattern indicates the single crystalline nature of the nanostructure.

The inset shows lattice fringes clearly. The distance between the neighboring fringes is 0.358 nm, which is close to the d -spacing of (110) plane of rutile TiO_2 ($d_{(110)} = 0.325$ nm) [14]. The origin of observed larger interplanar spacing is unclear. Similar phenomena were reported by other researchers [15, 16]. Factors such as measurement errors, existence of possible impurities, surface relaxation [17], and the nature of substrate materials could all play a role. The growth direction of the nanostructure is around 17° away from [110], which is close to the [210] direction. In short, the as-synthesized nanostructures were characterized to be single crystalline rutile TiO_2 with the preferred growth direction close to the [210].

Several growth controlling factors, including catalytic materials, growth temperature and growth duration, were investigated systematically.

(i) *Catalytic Materials.* Figure 2a, b shows the nanostructures synthesized without and with the catalytic material Ni at 850°C for 60 min, respectively. It is obvious that the growth of TiO_2 nanostructures can be greatly enhanced by using the catalytic material. The optimum thickness of catalytic material film is ~ 2 nm. Thicker or thinner films produced less 1D nanostructures. When employing different catalytic materials in control experiments, the effectiveness of them was found to be in the order of $\text{Ni} > (\text{Au}, \text{Ag}) > (\text{Pd}, \text{Pt})$. While a catalytic material was used in syntheses, it can be detected from the tips of most nanostructures by the TEM/EELS observation.

(ii) *Growth Temperature.* The center position temperature of the tube furnace was varied from 750 to 1050°C with an interval of 100°C while the reaction time was kept as 60 min. Figure 2c, d shows the nanostructures synthesized at 750 and 1050°C , respectively. At higher temperatures, longer, thicker, straighter, and more heavily populated nanowires can be grown.

(iii) *Growth Duration.* Reaction time was varied from 15 to 120 min while the center position temperature of the tube furnace was kept at 950°C . Figure 2e, f shows the nanostructures synthesized in 15 and 120 min, respectively. Prolonged reaction time produced longer and slightly thicker TiO_2 nanostructures. In short, the growth of TiO_2 1D nanostructures can be enhanced by using catalytic materials, higher reaction temperature and longer reaction time.

The aforementioned experimental results raise a question: how many growth mechanisms are involved in the growth of TiO_2 nanostructures from Ni-coated Ti grids? The observation of Ni existing on the tips of most nanostructures suggests that the Vapor–Liquid–Solid (VLS) growth [18] might be the dominating mechanism. However, for the small amount of nanostructures without Ni on their tips and even structures directly grown from bare Ti grids, other growth mechanisms such as Vapor–Solid (VS)

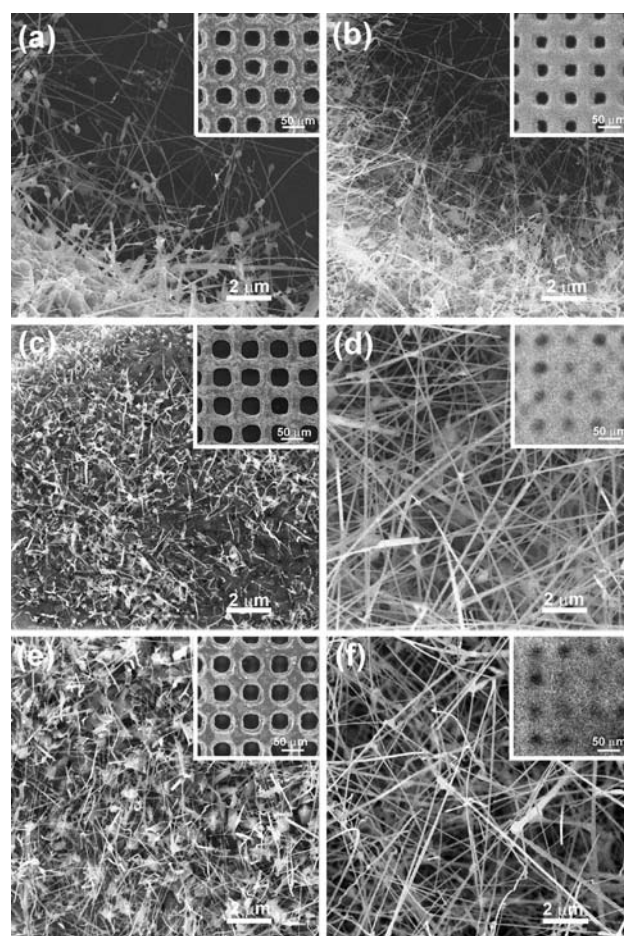


Fig. 2 SEM images of TiO_2 1D nanostructures synthesized at different conditions. Illustration of the effect of catalytic materials: the nanostructures were synthesized without (a) and with (b) catalytic material Ni at 850°C for 60 min. Illustration of the effect of reaction temperatures: the nanostructures were synthesized at 750°C (c) and 1050°C (d) for 60 min. Illustration of the effect of reaction time: the nanostructures were synthesized at 950°C for 15 min (e) and 120 min (f). Insets are low magnification images of as-synthesized nanostructures on Ti grids

and solid state oxidation growth could be involved [19]. Despite the various growth mechanisms, it is believed that the growth is governed by the chemical reaction: $\text{Ti} (\text{g or s}) + \text{O}_2 (\text{g}) \rightarrow \text{TiO}_2 (\text{s})$. Although our experiments were done in the Ar atmosphere, the oxygen could come from the leakage of air into the reaction chamber and other possible sources [12]. It was observed that the amount of O_2 plays a critical role in the formation of TiO_2 1D nanostructures. Deliberate introduction of 1 sccm O_2 into the reaction chamber suppressed the growth of TiO_2 nanostructures, but enhanced the formation of polycrystalline TiO_2 film. Similar results have been seen from growth of TiO_2 nanostructures directly from Ti foils using small organic molecules (e.g., acetone, water) as the O_2 source [9]. In order to quantify the exact amount of O_2

needed for growth of TiO_2 1D nanostructures from Ni-coated Ti grids, a new O_2 mass flow controller capable of controlling gas at 0.2 sccm level has been integrated into the tube furnace system recently. The results of these additional studies will be presented elsewhere.

Tensile Behavior of As-Synthesized TiO_2 1D Nanostructures

Nanoscale tensile loading [20–22] of individual TiO_2 1D nanostructures was performed with a custom-made nanomanipulator inside the vacuum chamber of a scanning electron microscope (JEOL JSM-7400F). In short, two Atomic Force Microscopy (AFM) chips were mounted on the two opposing linear positioning stages of the nanomanipulator. An AFM chip with long (compliant) cantilevers (MikroMasch, Inc.; Chip NSC 12, lengths 350 and 300 μm , nominal force constants 0.3 and 0.5 N/m, respectively) was mounted on the X–Y linear stage, and an AFM chip with short (stiff) cantilevers (MikroMasch, Inc.; Chip NSC 12, lengths 90 and 110 μm , nominal force constants 14.0 and 7.5 N/m, respectively) was mounted on the opposing Z linear stage together with the TiO_2 1D nanostructures source (i.e., a Ti grid with 1D nanostructures on it) (Fig. 3a). Through nanomanipulation, an individual TiO_2 1D nanostructure was picked up from the source and clamped between the two opposing AFM tips with the electron beam induced deposition method (Fig. 3b). The long (compliant) cantilever, served as the force-sensing element, was then gradually moved away from the short (stiff) cantilever by actuating a piezoelectric bender (Noliac A/S.; CMBP 05) with a dc voltage. An increasing tensile load was thus applied to the nanostructure until it fractured. In our current experimental approach, the applied tensile load and strain in the nanostructure were not directly obtained during the loading process. During the test, the tensile load was increased in discrete steps and SEM images at each loading step were acquired. The applied tensile load and strain in nanostructure at each loading step were obtained later based on the corresponding force-sensing cantilever deflection and nanostructure elongation from image analysis [20, 21]. The bending stiffness of the force-sensing AFM cantilever was calibrated with a resonance method in vacuum right before the test [23].

Six nanoscale tensile tests were successfully performed on four individual TiO_2 1D nanostructures, with the sample #2 being repeatedly tested three times. The experimental results are summarized in Table 1. Based on the stress–strain relationships obtained, all these nanostructures appeared to fracture in a brittle manner, and the failure strain ranged from 0.6 to 4.7%. SEM observation of the nanostructure fragments did not reveal any visible necking.

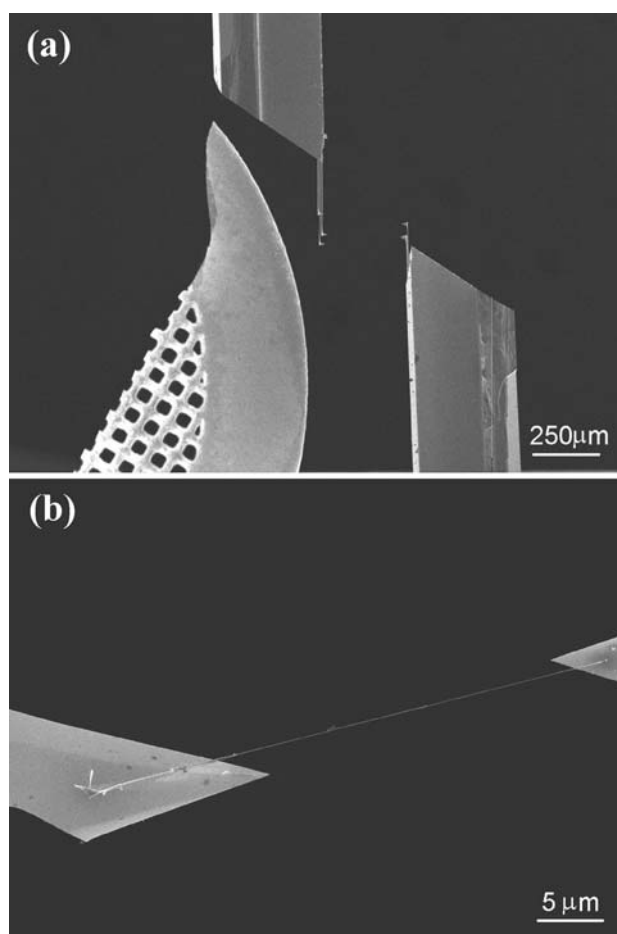


Fig. 3 **a** Low magnification SEM image of the nanoscale tensile test experiment configuration; **b** SEM image of a TiO_2 1D nanostructure clamped between two AFM cantilever tips under a tensile load

The fracture strength of the TiO_2 nanostructure ranged from 0.3 to 4.2 GPa with an average value of ~ 1.4 GPa. The corresponding Young's modulus obtained from linear data fitting of the stress–strain curve ranged from 47 to 89 GPa, with an average value of ~ 56 GPa. Sample #3 was noticed to have a smallest value of diameter but a highest value of Young's modulus, indicating a possible size effect [24].

The sample #2 and its fragments were repeatedly loaded three times, with higher breaking force required for each successive test as well as increased failure strain. Such trend has been observed in our previous multiple tensile loading studies on individual multi-wall carbon nanotubes [21]. Considering that a nanostructure under uniaxial tension should fail at the “critical flaw” along its length, the resulting nanostructure fragments should contain less significant defects than the original one, and should thus possess a higher fracture strength. The Young's modulus values for the sample #2 obtained from linear fit of the three stress–strain curves are very close, as expected.

Table 1 Tensile testing results on four TiO₂ 1D nanostructures with sample #2 repeatedly tested three times

Sample #	Diameter (nm)	Length (μm)	Breaking force (μN)	Tensile strength (MPa)	Failure strain (%)	Young's modulus (GPa)
1	52	7.85	1.57	740	1.5	52
2_1	47	17.13	0.51	290	0.6	48
2_2	47	14.60	0.83	460	1.0	48
2_3	47	9.68	1.94	1,170	2.5	47
3	28	15.02	2.58	4,200	4.7	89
4	66	38.82	7.70	2,250	3.9	54

For a tetragonal crystal system of class 4/mnm, the Young's modulus (E) along a unit vector $[l_1 l_2 l_3]$ can be expressed as [25]

$$\frac{1}{E_{[l_1 l_2 l_3]}} = (l_1^4 + l_2^4)S_{11} + l_3^4 S_{33} + l_1^2 l_2^2 (2S_{12} + S_{66}) + l_3^2 (1 - l_3^2) (2S_{13} + S_{44}) \quad (1)$$

where S_{ij} (i, j run from 1 to 6) are stiffnesses and can be converted from compliances (i.e., elastic constants, C_{ij}) [25]. Using the available elastic constants for rutile TiO₂ [26], the Young's modulus of [210] direction was calculated to be ~239 GPa, which is higher than the experimental value (~56 GPa). Literature search shows that lower Young's moduli for 1D nanostructures have been reported [27–30]. For example, the Young's moduli of ZnO 1D nanostructures were measured to be 29 ± 8 GPa [28] and 31.1 ± 1.3 GPa [29], which are significantly lower than the calculated Young's modulus of bulk ZnO ($E_{\text{bulk ZnO } [0001]} = 140$ GPa [24]). Despite of measurement errors, surface stress might be the key reason causing the lower modulus [31]. Lee et al. reported the three-point bending of anatase polycrystalline TiO₂ nanofibers, the average elastic modulus of these fibers (~75.6 GPa) was found to be incomparable with the calculated value for bulk anatase TiO₂ (e.g., $E_{\text{bulk anatase } [100]} = 192$ GPa) [32], mainly due to the polycrystalline nature of the nanofibers and inherent error associated with the testing method [30]. While the causes of our measured lower modulus of TiO₂ 1D nanostructures need further investigation, the observed larger interplanar spacing might be one reason.

Conclusions

In summary, a simple synthetic process to produce TiO₂ 1D nanostructures by heating Ni-coated Ti grids has been described. The as-synthesized 1D nanostructures were characterized to be single crystalline rutile TiO₂, with the preferred growth direction close to [210]. Tensile behavior of individual 1D nanostructures was studied by nanoscale tensile testing with a nanomanipulator in an scanning electron microscope. The measured Young's modulus was

~56 GPa, lower than the value for bulk TiO₂. The reported synthetic technique could facilitate the in situ growth study of 1D nanostructures by TEM. The mechanical characterization of TiO₂ 1D nanostructures provides useful information for future device integration of these nanoscale building blocks.

Acknowledgments T. Xu appreciates the support of the start-up fund and junior research grant at the University of North Carolina at Charlotte (UNC Charlotte). W. Ding appreciates the support of the start-up fund at Clarkson University. We are grateful to the Center for Optoelectronics and Optical Communications at UNC Charlotte, the Center for Advanced Materials Processing at Clarkson, and NUANCE center at Northwestern University for supplying multi-user facilities used for this work.

References

1. X. Chen, S.S. Mao, J. Nanosci. Nanotechnol. **6**, 906 (2006)
2. A. Ghicov, P. Schmuki, Chem. Commun. **20**, 2791 (2009)
3. K.H. Yu, J.H. Chen, Nanoscale Res. Lett. **4**, 1 (2009)
4. J.-M. Wu, H.C. Shih, W.-T. Wu, Nanotechnology **17**, 105 (2006)
5. J.-C. Lee, K.-S. Park, T.-G. Kim, H.-J. Choi, Y.-M. Sung, Nanotechnology **17**, 4317 (2006)
6. J.M. Baik, M.H. Kim, C. Larson, X.H. Chen, S.J. Guo, A.M. Wodtke, M. Moskovits, Appl. Phys. Lett. **92**, 242111 (2008)
7. J.J. Wu, C.C. Yu, J. Phys. Chem. B **108**, 3377 (2004)
8. C.A. Chen, Y.M. Chen, A. Korotcov, Y.S. Huang, D.S. Tsai, K.K. Tiong, Nanotechnology **19**, 075611 (2008)
9. X. Peng, J. Wang, D.F. Thomas, A. Chen, Nanotechnology **16**, 2389 (2005)
10. K.F. Huo, X.M. Zhang, L.S. Hu, X.J. Sun, J.J. Fu, P.K. Chu, Appl. Phys. Lett. **93**, 013105 (2008)
11. J. Park, Y. Ryu, H. Kim, C. Yu, Nanotechnology **20**, 105608 (2009)
12. S.S. Amin, A.W. Nicholls, T.T. Xu, Nanotechnology **18**, 445609 (2007)
13. G.M. Begun, C.E. Bamberger, Appl. Spectrosc. **43**, 134 (1989)
14. JCPDS Database, PDF#21-1276, Materials Data, Inc
15. N.P. Kobayashi, S.Y. Wang, C. Santori, R.S. Williams, Appl. Phys. A Mater. **85**, 1 (2006)
16. L. Gao, R.L. Woo, B. Liang, M. Pozuelo, S. Prihodko, M. Jackson, N. Goel, M.K. Hudait, D.L. Huffaker, M.S. Goorsky, S. Kodambaka, R.F. Hicks, Nano Lett. **9**, 2223 (2009)
17. U. Diebold, Surf. Sci. Rep. **48**, 53 (2003)
18. R.S. Wagner, W.C. Ellis, Appl. Phys. Lett. **4**, 89 (1964)
19. Y.N. Xia, P.D. Yang, Y.G. Sun, Y.Y. Wu, B. Mayers, B. Gates, Y.D. Yin, F. Kim, Y.Q. Yan, Adv. Mater. **15**, 353 (2003)

20. W.Q. Ding, L. Calabri, X.Q. Chen, K.M. Kohhaas, R.S. Ruoff, *Comp. Sci. Technol.* **66**, 1112 (2006)
21. W. Ding, L. Calabri, K.M. Kohlhaas, X. Chen, D.A. Dikin, R.S. Ruoff, *Exp. Mech.* **47**, 25 (2007)
22. W.Q. Ding, Z.Y. Guo, R.S. Ruoff, *J. Appl. Phys.* **101**, 034316 (2007)
23. J.E. Sader, I. Larson, P. Mulvaney, L.R. White, *Rev. Sci. Instrum.* **66**, 3789 (1995)
24. C.Q. Chen, Y. Shi, Y.S. Zhang, J. Zhu, Y.J. Yan, *Phys. Rev. Lett.* **96**, 075505 (2006)
25. J.F. Nye, *Physical Properties of Crystals* (Oxford University Press, Oxford, 1985), pp. 143–149
26. D.G. Isaak, J.D. Carnes, O.L. Anderson, H. Cynn, E. Hake, *Phys. Chem. Miner.* **26**, 31 (1998)
27. X.D. Bai, P.X. Gao, Z.L. Wang, E.G. Wang, *Appl. Phys. Lett.* **82**, 4806 (2003)
28. J.H. Song, X.D. Wang, E. Riedo, Z.L. Wang, *Nano Lett.* **5**, 1954 (2005)
29. H. Ni, X.D. Li, *Nanotechnology* **17**, 3591 (2006)
30. S.-H. Lee, C. Tekmen, W.M. Sigmund, *Mater. Sci. Eng. A* **398**, 77 (2005)
31. G.F. Wang, X.D. Li, *Appl. Phys. Lett.* **91**, 231912 (2007)
32. I. Gheewala, R. Smith, S.D. Kenny, *J. Phys. Condens. Matter* **20**, 354010 (2008)